Leadership in Sustainable Infrastructure
Leadership en Infrastructures Durables

Vancouver, Canada
May 31 – June 3, 2017/ *Mai 31 – Juin 3, 2017*

NUMERICAL AND ANALYTICAL APPROACHES TO MODEL COVER CRACKING OF RC STRUCTURES DUE TO CORROSION

Roshan, Arman[1,4], Martín-Pérez, Beatriz[2], and Noël, Martin[3]
[1,2,3] University of Ottawa, Canada
[4] roshan.arman@gmail.com

Abstract: In this study, two approaches are presented to model corrosion-induced crack propagation. The first approach is a finite-difference solution which treats cracked concrete as an orthotropic material. This approach models tension softening assuming smeared cracking for concrete in tension and considers concrete as an inelastic material in compression. A program was developed using MATLAB to solve the problem numerically. The second approach is an analytical solution based on a thick-walled cylinder analogy. This approach simplifies the problem by considering the partially cracked concrete cover as a combination of an outer un-cracked thick wall cylinder and an inner cracked concrete cylinder. Concrete is considered as an elastic, brittle material, and shear stresses between the cracked and un-cracked cylinders are neglected. Both models take into the account the compressibility of the corrosion products and the available space within the cracks for corrosion products to disperse. The results obtained using each approach are compared against each other as well as against experimental results. In general, the observed trends from experimental measurements were captured by the two modelling approaches used. Advantages and disadvantages of each are discussed.

1 Introduction

Reinforcement corrosion is the most common mode of degradation in reinforced concrete (RC) structures, comprising 55% of all deterioration cases in Europe (Tilly 2007). Due to excessive use of de-icing salts, degradation induced by reinforcement corrosion is even more prominent in RC structures in Canada. Corrosion is an electrochemical process in which iron, water, and oxygen are consumed to produce rust products that occupy a greater volume than the parent iron. The ratio of rust products to parent iron is called the rust expansion coefficient (R_v), which ranges from 2.08 to 6.4 (Caré et al. 2008). This expansion leads to a buildup of pressure at the reinforcement and concrete interface. Being weak in tension, the concrete cover will eventually crack to release the pressure generated, thereby providing more space to the rust products. As the corrosion process continues the pressure will build up further, leading cracks to eventually propagate to the surface. If unattended, crack widening, formation of other cracks, and spalling of the concrete cover will ensue.

Since cracks due to corrosion form parallel to the reinforcement, the cracked concrete cover is usually represented by two-dimensional models. Two modelling approaches and their results are discussed in this paper. Both models are two-dimensional and employ the thick-walled cylinder analogy as the basis for idealizing the phenomenon. Therefore, they only consider the concrete cover within the thick-walled cylinder around the corroded steel to be effective.

2 Numerical Approach

In this first approach, it is assumed that crack planes are perpendicular to planes of maximum normal tensile strain. The direction of principal strains has been assumed to coincide with the direction of principal stresses, which correspond to the radial (r) and hoop directions (θ), respectively (Figure 1 (a)). Therefore, cracks propagate radially towards the concrete surface. Due to the assumption of axisymmetry in the thick-wall cylinder analogy, it is further assumed that radial cracks are smeared throughout the concrete ring. Smeared cracking is useful for representing concrete behaviour in tension, especially at the initial stages of corrosion when several micro-cracks have formed and none of the cracks are distinctly larger than the others. Consequently, the concrete cover has been assumed as an orthotropic material where the material axes are oriented along the r and θ directions. The constitutive relations that define concrete's behaviour in tension and compression are formulated in terms of average stresses and average strains, which are related by secant moduli along the principal directions (Pantazopoulou and Papoulia 2001). The axisymmetry assumption also cancels out shear stresses between elements. A finite-deference program has been developed using MATLAB to solve the formulated mathematical problem.

2.1 Modelling the Confinement Capacity of the Concrete Cover

Starting with force equilibrium along the radial direction and compatibility of deformations of any element within the thick-walled cylinder (Figure 1 (a)), Equations 1 and 2 can be written:

[1] $$\sigma_r + \frac{d\sigma_r}{dr} r - \sigma_\theta = 0$$

[2] $$\varepsilon_r = \frac{du}{dr},\ \varepsilon_\theta = \frac{u}{r}$$

where ε_r and ε_θ are radial and hoop strains, respectively, σ_r and σ_θ are the corresponding radial (compressive) and hoop (tensile) stresses, r is the radius of the concrete ring where stress or strain is being calculated, and u is the radial displacement at r. As shown in Figure 1, r_b is the rebar radius, and c is the cover depth.

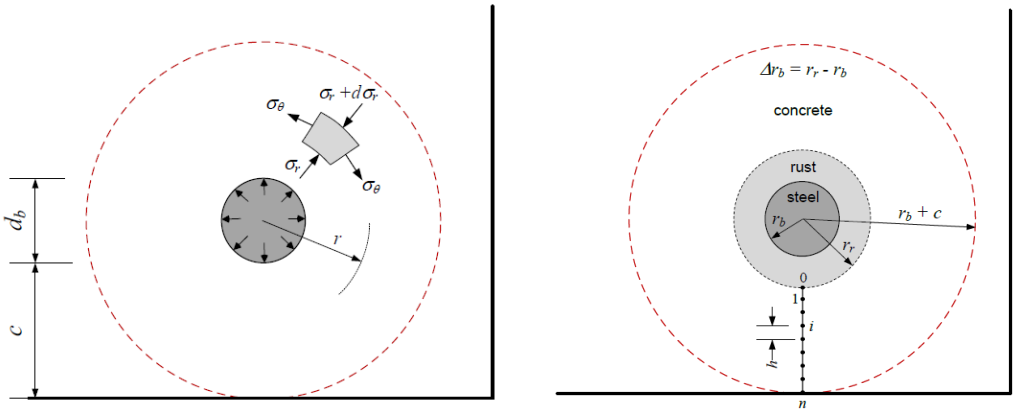

(a) (b)

Figure 1: (a) Equilibrium and compatibility of any element within the thick-walled cylinder; (b) Numerical discretization of concrete cover along radial direction

Assuming the concrete behaves as an orthotropic material, this problem is governed by a second-order linear differential equation (Equation 3), which describes the radial deformation (u) at a certain radial coordinate (r):

[3] $$\frac{d^2u}{dr^2} + \frac{1}{r} \times \frac{du}{dr} - \frac{E_\theta}{E_r} \times \frac{u}{r^2} = 0$$

where E_θ and E_r are the secant moduli in tension and compression, respectively.

The boundary conditions are:

[4] $$u(r = r_r) = \Delta r_b$$

[5] $$\sigma_r(r = r_b + c) = 0$$

where Δr_b is the uniform radial displacement at the reinforcement and concrete interface (inner boundary of the thick-walled cylinder) imposed by the corrosion.

The governing differential equation (Equation 3), along with the boundary conditions (Equations 4 and 5), can be solved numerically by discretizing the concrete cover into n+1 equally spaced (h) points $(r_r, r_1, r_2, \dots, r_n)$ and using the first central finite difference approximations at each discrete point (Pantazopoulou and Papoulia 2001) (Figure 1 (b)).

2.2 Modelling the Compressibility of the Rust

The model presented also accounts for the compressibility of corrosion products by considering the bulk modulus of the rust (Equation 6):

[6] $$\Delta V_{rp} = -\frac{V_{rr} \times P}{B_r}$$

where ΔV_{rp} is the volume of corrosion products that are compressed due to the pressure build-up, V_{rr} is the expected volume of corrosion products if they were allowed to expand freely, B_r is the bulk modulus of corrosion products, and P is the pressure at the reinforcement/concrete interface. A bulk modulus of 0.5 GPa has been used to consider compressibility of corrosion products (Konopka 2005).

2.3 Accounting for the Volume of the Cracks

As the concrete cover cracks due to corrosion-induced pressure, the cracks also provide some space to be filled by the corrosion products. This space is in addition to that provided by the displaced inner boundary of the thick-walled cylinder. Assuming that the cracks are triangular, the volume of corrosion products within the corrosion-induced cracks per unit length of the rebar, V_{cr}, can be estimated from Equation 7:

[7] $$V_{cr} = \frac{1}{2} C_v \times w_{cr} \times (r_c - r_r)$$

where r_c and r_r are the crack and rust fronts, respectively, w_{cr} is the total crack width at the reinforcement/concrete interface, and C_v is a crack volume coefficient.

According to Molina et al. (1993), the crack width w_{cr} can be estimated by Equation 8 where smeared cracking has been assumed:

[8] $$w_{cr} = 2\pi r(\varepsilon_\theta - \varepsilon_{cr}), \qquad \varepsilon_{cr} = \frac{f_t'}{E_0}$$

where f_t' and E_0 are the tensile strength and the initial Young's modulus of the concrete, respectively. For comparison with experimental results, the mechanical parameters f_t' and E_0 were taken from expressions proposed by the CEB-FIP Model Code (2010) unless measured values were reported.

Since not all of the space within the cracks is likely to be filled by corrosion products (Merino 2014), it is assumed here that they occupy only 50% of the crack volume; therefore, C_v has been assumed equal to 0.5.

2.4 Concrete Constitutive Behaviour

It has been observed in experimental tests that tensile stress in concrete at the location of a crack does not drop to zero immediately following crack initiation (Evans and Marathe 1968). Instead, the tensile stress gradually decreases from its peak value (i.e., tensile strength) as total tensile strain increases. This post-peak behaviour is known as strain softening. A nonlinear tension softening model proposed by Hordijk (1991) has been used here to model the tension softening of the concrete cover (Figure 2 (a)).

A combination of Hognestad parabola and a compression softening model introduced by Vecchio and Collins (1986) has been used to model concrete in compression (Figure 2 (b)).

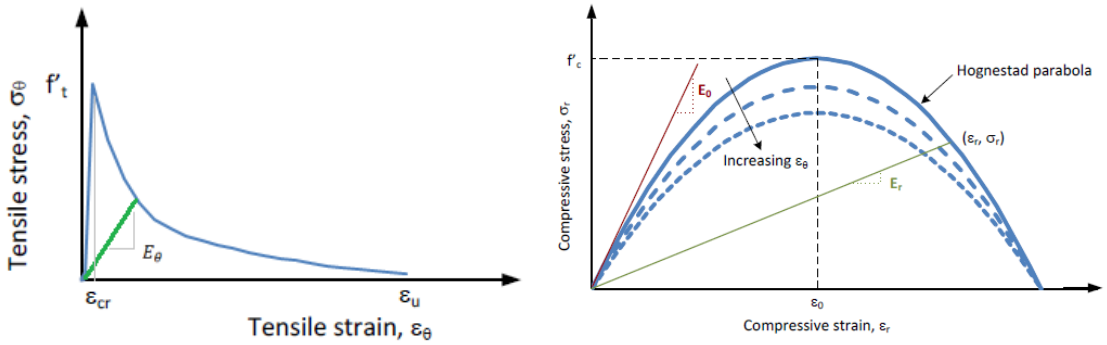

(a) (b)

Figure 2: Stress-strain relationship for concrete in tension (a), and compression (b)

3 Analytical Approach

3.1 Assumptions and Analogy

The second modelling approach simplifies the problem by assuming the following:

- The concrete cover, previously modelled as a single thick-walled cylinder, is now idealized as two cylinders: an outer un-cracked cylinder and an inner cracked cylinder (Figure 3).
- Concrete is an elastic material.
- Concrete is a brittle material with no tension softening.
- Only radial compressive stresses are transferred between the two cylinders.

Consequently, the radial displacement at the boundary (u_1) of the two cylinders can be found using Equation 9 (Figure 3):

[9] $$\varepsilon_{cr} = \frac{u_1}{r_c} \quad \rightarrow \quad u_1 = r_c \times \varepsilon_{\theta=}\varepsilon_{cr}$$

The radial compressive stress at the boundary of the two cylinders σ_b can be found using Equation 10 (Timoshenko 1956):

[10] $$\sigma_b = \frac{u_1 E_c\left((c+r_b)^2 - r_c^2\right)}{r_c\left[(1-\nu_c)r_c^2 + (1+\nu_c)(c+r_b)^2\right]}$$

where ν_c and E_c are the Poisson's ratio and Young's modulus of the concrete cover.

Consequently, the internal pressure at the interface between the reinforcement and the concrete cover can be calculated by Equation 11 where tension softening is neglected:

[11] $$P = \sigma_b \times \frac{r_c}{r_r}$$

Equation 12 determines the radial compression (u_2) of the cracked cylinder subjected to the radial compressive pressure:

[12] $$u_2 = \int_{r_r}^{r_c} \varepsilon_r dr \quad \rightarrow \quad u_2 = \frac{r_c \sigma_b}{E_c} \times \int_{r_r}^{r_c} \frac{1}{r} dr \quad \rightarrow \quad u_2 = \frac{r_c \sigma_b}{E_c} \times \ln \frac{r_c}{r_r}$$

Accordingly, the radial movement of the inner boundary of the cracked concrete is obtained from Equation 13 (Figure 3):

[13] $$\Delta r_b = u_1 + u_2$$

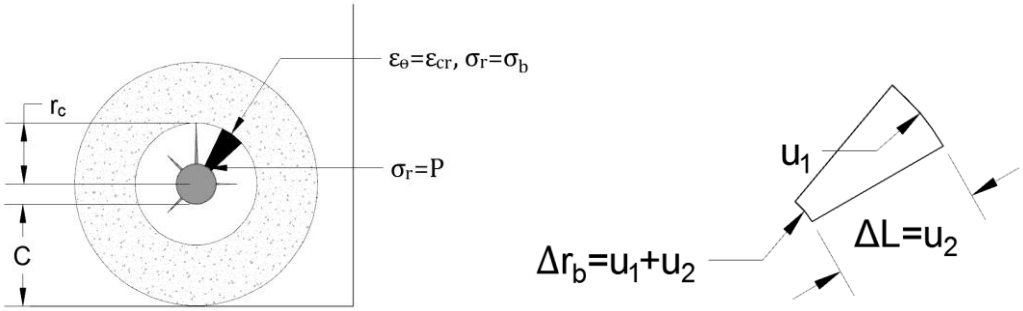

Figure 3: Analytical Approach

The analytical approach also considers the available space within the corrosion-induced cracks. However, here it is assumed that all of the available space within the triangular shaped corrosion-induced cracks will be filled by the corrosion products (i.e. C_v = 1.0). Since the model does not account for tension softening, Equation 8 is simplified to Equation 14:

[14] $$w_{cr} = 2\pi r(\varepsilon_\theta)$$

[15] $$\Delta V_{cr} = \frac{1}{2} \times w_{cr} \times (r_c - r_r) = \pi \times \Delta r_b \times (r_c - r_r)$$

where ΔV_{cr} denotes the available space within the cracks.

The analytical approach considers the compressibility of the corrosion products in the same way as the numerical model by using the bulk modulus of the rust. Therefore, the total volume of the corroded rebar can be calculated from Equation 16:

[16] $$\Delta V_s = \frac{\pi(r_r^2 - r_b^2) + \Delta V_{cr}}{R_v\left(1 - \frac{P}{B_r}\right) - 1}$$

The corresponding attack penetration, x, which refers to the radius of the original rebar minus the radius of the corroded rebar, can be calculated from Equation 17:

[17] $$x = r_b - \left(r_b^2 - \frac{\Delta V_s}{\pi}\right)^{\frac{1}{2}}$$

The critical attack penetration refers to the attack penetration at the time when a crack reaches the concrete surface.

4 Results and Comparison

The results obtained using both approaches were compared against reported experimental results. It should be noted that experimental studies usually report the time or the attack penetration once the first hairline crack is visible to the naked eye, generally corresponding to an actual crack width of at least 0.05 mm. This is referred to herein as the visual critical attack penetration. The visual critical attack penetration is about

2-3 times larger than the actual critical attack penetration (Merino 2014). Other researchers have compared results obtained from their analytical or numerical models (critical attack penetration) against the visual critical penetration reported by experimental tests. In the present study, reported experimental results from the literature have been compared against either the visual critical attack penetrations (crack width of 0.05 mm) using the numerical approach, or the actual critical attack penetration using the analytical approach. Table 1 compares the assumptions and parameters used in each approach.

Table 1: Comparison of the Numerical and the Analytical Approaches

	Numerical Approach	Analytical Approach
Rust Expansion Coefficient (R_v)	2.75	2.00
Crack Volume Coefficient (C_v)	0.50	1.00
Compared against:	Visual Critical Attack Penetration	Actual Critical Attack Penetration
Concrete in Compression	Hognestad parabola and a compression softening model	Linear Elastic
Concrete in Tension	Non-Linear Tension Softening	No Tension Softening

4.1 Detailed Results

The numerical and analytical models presented were used to simulate the experimental results of specimen SII_1 reported by Vu et al. (2005), wherein the bar diameter $d_b = 16\ mm, c = 50\ mm, f_t' = 3.94\ MPa,\ f_c' = 42.25\ MPa, E_c = 34.3\ GPa,\ v_c = 0.2$. Figure 4 plots the resulting rust front (r_r), radius of the corroded rebar $(r_b - x)$, internal pressure, crack front (r_c), perimeter hoop strain, and crack width against time. The attack penetration (x) has been related to time by Faraday's law, where the corrosion current density (i_{cor}) is assumed equal to 100 $\mu A/cm^2$.

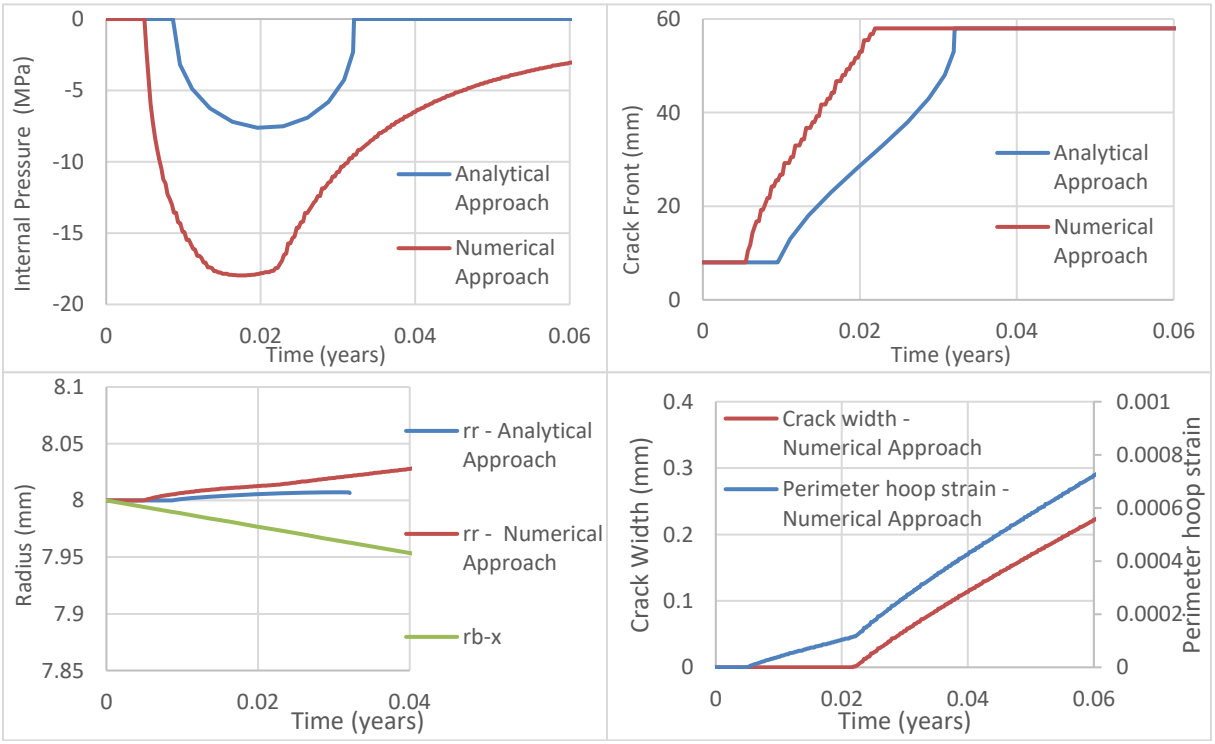

Figure 4: Comparison of the numerical and analytical results for specimen SII_1 taken from Vu et al. (2005)

The analytical approach is not able to provide any results for the rust front after the crack propagates to the surface.

4.2 Critical Attack Penetration

Figure 5 plots the ratio of the numerical results to the experimental results obtained from the literature. Figure 6 plots the ratio of the analytical results to the experimental results. Figure 7 plots the numerical and experimental results against cover-to-diameter ratio. Figure 8 plots the analytical and experimental results against cover-to-diameter ratio.

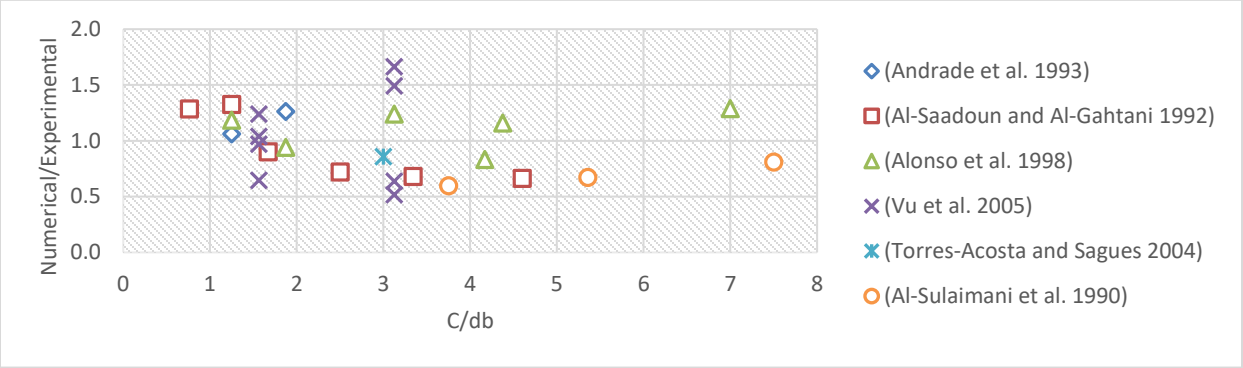

Figure 5: Comparison of numerical results for visual critical attack penetration against experimental (visual) critical attack penetration

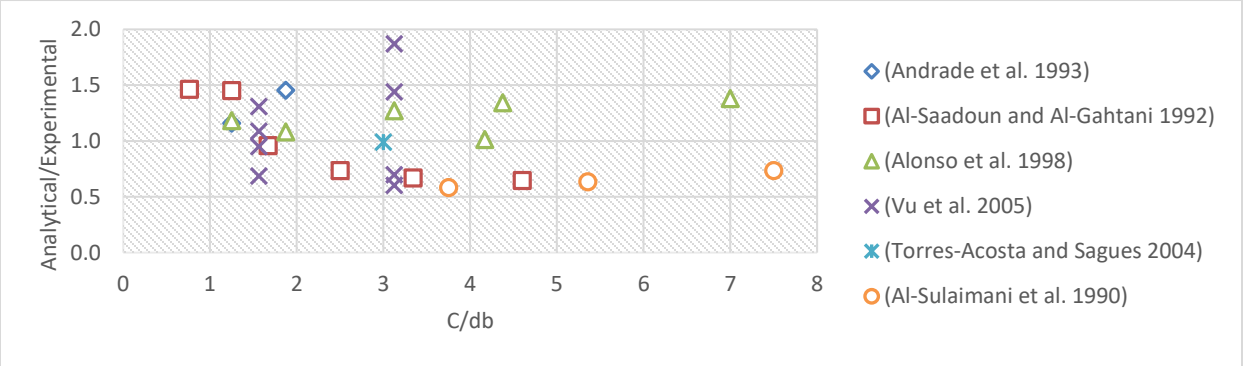

Figure 6: Comparison of analytical results for actual critical attack penetration against experimental (visual) critical attack penetration

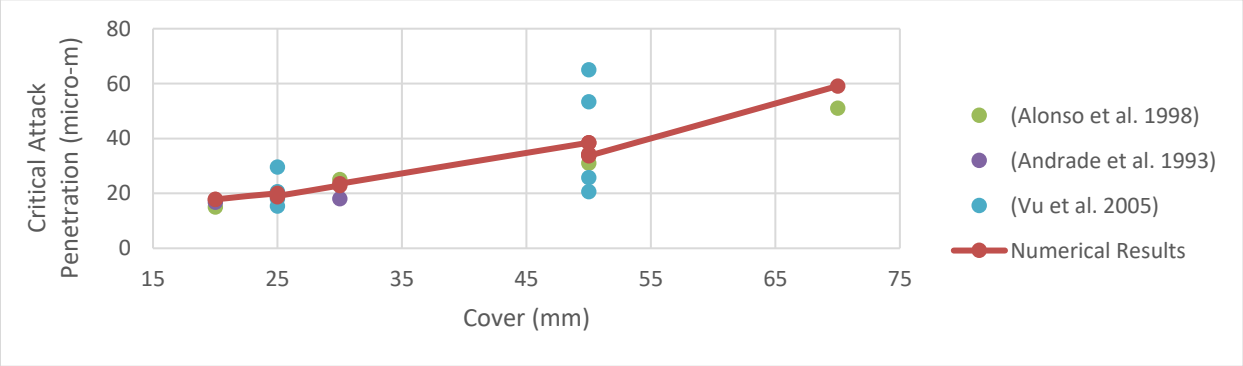

Figure 7: Numerical and experimental results of (visual) critical attack penetration for diameter of 16mm

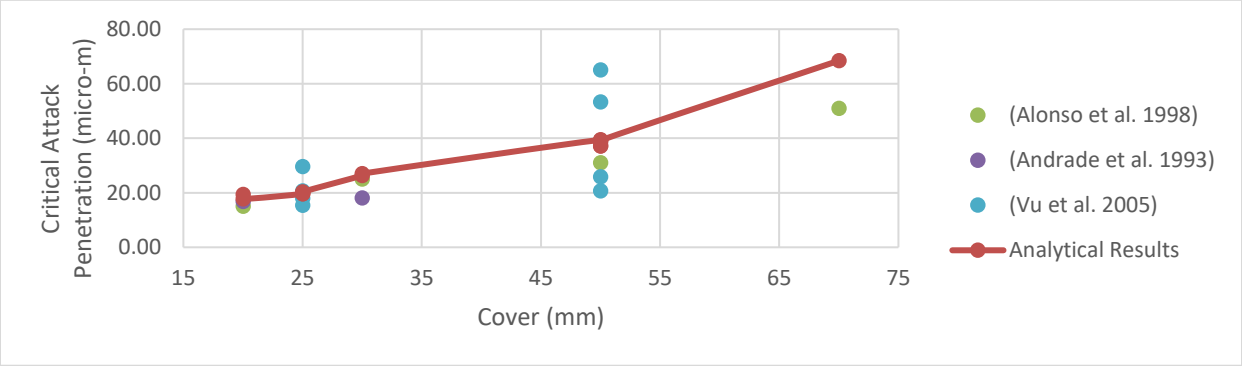

Figure 8: Analytical and experimental results of critical attack penetration for diameter of 16mm

It can be observed that the numerical and analytical results are very similar. Figures 7 and 8 demonstrate the high variability in the experimental results. This variability may be largely attributed to the difference in the actual rust expansion coefficients produced in the different experimental tests, which are very difficult to measure and usually not reported.

4.3 Maximum Pressure and Critical Crack Depth

The maximum internal pressure (P_{max}) refers to the maximum pressure experienced at the reinforcement/concrete interface during the corrosion process. In other words, P_{max} is the maximum pressure which can be applied at the interface before the concrete cover fails (Figure 9 (a)). According to Williamson and Clark (2000), Morinaga (1988) tested hollow cylindrical concrete specimens by applying an internal pressure (simulating corrosion-induced pressure); (c/d_b) ranged from 1.5 to 3.5 in his tests. There is good agreement between the results calculated using the empirical equation presented by Morinaga and the results calculated by the numerical approach within the range of Morinaga's tests. However, both sets of results diverge as c/d_b increases above 3.5. Williamson and Clark (2000) performed similar tests and suggested that f_t' has no effect on the maximum pressure, which contradicts the findings reported herein.

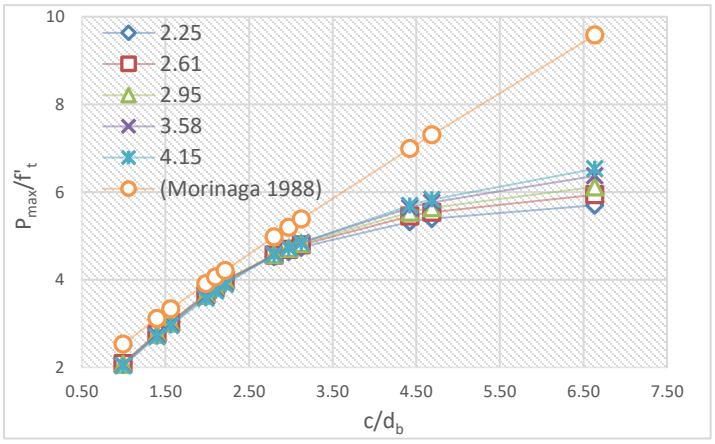

Figure 9: Comparison of maximum internal pressure found by the numerical model and that proposed by Morinaga (1988)

The analytical approach generally underestimated the maximum pressure in comparison with both the numerical approach and the empirical equation given by Morinaga (1988). The analytical model estimates the maximum pressure to be around 40% of the predicted values from the Morinaga equation (Figure 4).

The critical crack depth is the crack front corresponding to the maximum internal pressure (P_{max}) (Tepfers 1979). The ratio of the critical crack depth to the concrete cover depth is referred to as the critical crack depth ratio (R_{oc}). Figure 10 plots critical crack depth ratios found by the numerical approach against cover to diameter ratio.

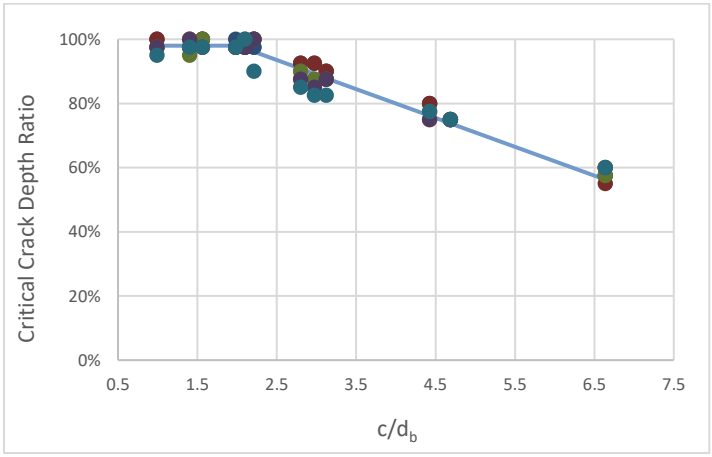

Figure 10: Critical crack depth ratio for different cover-to-rebar diameter ratios

The critical crack depth ratio was constant for c/d_b ratios less than 2.3, but decreased linearly for c/d_b larger than 2.3. This observation is not in agreement with the Tepfers (1979) equation, which provides similar critical crack depth ratios as those found using the analytical approach discussed in this paper.

The effect of poisson's ratio, maximum aggregate size, and bulk modulus were found to be negligible on the maximum pressure and the critical crack front. The effect of f_t' was found to be negligible on the critical crack front as well.

5 Conclusions

Although both approaches can capture the trend observed by the reported experimental results, the accuracy of predictions compared with individual experiments in the literature present considerable scatter. This may be attributed to following reasons:

- Although rust expansion and crack volume coefficients are not the same in all the experimental tests, constant coefficients were used in lieu of more accurate values.
- Small differences in actual crack widths corresponding to the visual critical attack penetration compared to the assumed value of 0.05 mm introduce major differences in the results.
- The effect of parameters which are not considered in the models such as the water to cement ratio (i.e. porosity) of the concrete.

Since both approaches provide similar results for the (visual) critical attack penetrations, the analytical approach may be used to predict the critical attack penetration due to its ease of use.

However, since the numerical approach employs more realistic parameters and assumptions in comparison to the analytical model, it may be used to estimate the maximum pressure, critical attack penetration or to simulate the propagation process with more accuracy.

References

Al-Sulaimani, G J, M Kaleemullah, I A Basunnul, and A Al-Musallam Rasheeduzzafar. 1990. “Influence of Corrosion and Cracking on Bond Behaviour and Strength of Reinforced Concrete Members.” *ACI Structural Journal* 87 (2): 220–31. http://www.concrete.org/PUBS/JOURNALS/OLJDetails.asp?Home=SJ&ID=2732.

Al-Saadoun, S. S., and A. S. Al-Gahtani. 1992. “Corrosion Cracking in Relation to Bar Diameter, Cover, and Concrete Quality.” *Journal of Materials in Civil Engineering* 4 (4). American Society of Civil Engineers: 327–42. doi:10.1061/(ASCE)0899-1561(1992)4:4(327).

Alonso, C., C. Andrade, J. Rodriguez, and J. M. Diez. 1998. “Factors Controlling Cracking of Concrete Affected by Reinforcement Corrosion.” *Materials and Structures* 31 (7): 435–41. doi:10.1007/BF02480466.

Andrade, C., C. Alonso, and F. J. Molina. 1993. “Cover Cracking as a Function of Bar Corrosion: Part I-Experimental Test.” *Materials and Structures* 26 (8): 453–64. doi:10.1007/BF02472805.

Caré, S., Q.T. Nguyen, V. L’Hostis, and Y. Berthaud. 2008. “Mechanical Properties of the Rust Layer Induced by Impressed Current Method in Reinforced Mortar.” *Cement and Concrete Research* 38 (8–9): 1079–91. doi:10.1016/j.cemconres.2008.03.016.

Evans, R. H., and M. S. Marathe. 1968. “Microcracking and Stress-Strain Curves for Concrete in Tension.” *Matériaux et Constructions* 1 (1): 61–64. doi:10.1007/BF02479001.

fib – fédération internationale du béton. 2013. “Materials.” *Fib Model Code for Concrete Structures 2010*, 74–150. doi:10.1002/9783433604090.ch5.

Hordijk, Dirk Arend. 1991. “Local Approach to Fatigue of Concrete.” Delft University of Technology, The Netherlands.

Merino, B Sanz. 2014. “Experimental and Numerical Study of Cracking of Concrete due to Reinforcement Corrosion.” Universidad Politécnica de Madrid. http://oa.upm.es/30568/.

Molina, F. J., C. Alonso, and C. Andrade. 1993. “Cover Cracking as a Function of Rebar Corrosion: Part 2—Numerical Model.” *Materials and Structures* 26 (9): 532–48. doi:10.1007/BF02472864.

Pantazopoulou, S. J., and K. D. Papoulia. 2001. “Modeling Cover-Cracking Due To Reinforcement Corrosion in Rc Structures” 2 (April): 342–51.

Tepfers, Ralejs. 1979. “Cracking of Concrete Cover along Anchored Deformed Reinforcin Bars.” *Mag Concr Res* 31 (106): 3–12. doi:10.1680/macr.1979.31.106.3.

Tilly, Graham. 2007. “The Durability of Repaired Concrete Structures.” *IABSE Symposium Report* 93 (22). International Association for Bridge and Structural Engineering: 1–8. doi:10.2749/222137807796120030.

Torres-Acosta, Andres A., and Alberto A. Sagues. 2004. “Concrete Cracking by Localized Steel Corrosion-- Geometric Effects.” *Materials Journal* 101 (6): 501–7.

Vecchio, Frank J., and Michael P. Collins. 1986. “The Modified Compression-Field Theory for Reinforced Concrete Elements Subjected to Shear.” *ACI Journal Proceedings* 83 (2): 219–31. doi:10.14359/10416.

Vu, Kim, Mark G. Stewart, and John Mullard. 2005. “Corrosion-Induced Cracking: Experimental Data and Predictive Models.” *ACI Structural Journal* 102 (5): 719–26.

Williamson, S. J., and L. A. Clark. 2000. “Pressure Required to Cause Cover Cracking of Concrete due to Reinforcement Corrosion.” *Magazine of Concrete Research* 52 (6): 455–67. doi:10.1680/macr.2000.52.6.455.